Effects of Nonmigrating Diurnal Tides on the Na Layer in the Mesosphere and Lower Thermosphere

Jianfei Wu[1,2,3], Wuhu Feng[4,5], Xianghui Xue[1,2,3,6], Daniel R. Marsh[4], and John M. C. Plane[4]

[1]CAS Key Laboratory of Geospace Environment, School of Earth and Space Sciences, University of Science and Technology of China, Hefei, China
[2]Mengcheng National Geophysical Observatory, School of Earth and Space Sciences, University of Science and Technology of China, Hefei, China
[3]CAS Center for Excellence in Comparative Planetology, China
[4]School of Chemistry, University of Leeds, Leeds, UK
[5]National Centre for Atmospheric Science, University of Leeds, Leeds, UK
[6]Collaborative Innovation Center of Astronautical Science and Technology, 230026, Hefei, China

Correspondence: Xianghui Xue (xuexh@ustc.edu.cn)

Abstract. The influence of nonmigrating diurnal tides on Na layer variability in the mesosphere and lower thermosphere regions is investigated for the first time using data from the Optical Spectrograph and InfraRed Imaging System (OSIRIS) on the Odin satellite and Specified-Dynamic Whole Atmosphere Community Climate Model (SD-WACCM) with metal chemistry. The Na density from OSIRIS exhibits a clear longitudinal variation indicative of the presence of tidal components. Similar variability is seen in the SD-WACCM result. Analysis shows a significant relationship between the nonmigrating diurnal tides in Na density and the corresponding temperature tidal signal. Below 90 km, the three nonmigrating diurnal tidal components in Na density show a significant positive correlation with the temperature tides. Conversely, the phase mainly indicates a negative correlation above 95 km. Around the metal layer peak, the response of the Na density to a 1 K change in tidal temperature is estimated to be $120\,\mathrm{cm}^{-3}$.

1 Introduction

In the mesosphere and lower thermosphere (MLT), the atmospheric structure is significantly influenced by atmospheric tides with different spatial and temporal scale variations. Meteor-ablated metals such as sodium (Na), iron (Fe) and potassium (K) can be characterized as the optimal dynamical trace medium in the MLT (80-120 km in altitude), because their removal lifetimes are relatively long (Plane et al., 2015). The diurnal cycle of these meteoric atoms is driven by a complex combination of tidal forcing, chemistry and photochemistry in this region. Although several recent studies (e.g., Feng et al., 2013, 2015; Viehl et al., 2016; Yuan et al., 2019) have investigated the diurnal variation of the Na and Fe layers using a whole atmosphere chemistry-climate model, their findings mainly focused on photochemical influences. The mechanism of the diurnal variation still needs to be fully understood. This study addresses this gap in knowledge by examining the influence of nonmigrating tides, which previous research has not thoroughly explored.

20   Nonmigrating tides are of particular interest because they provide a unique opportunity to study energy, chemical, and dynamical transport mechanisms within the MLT region (Oberheide and Forbes, 2008; Smith, 2012; Ramesh and Smith, 2021; Li et al., 2022). Their stable wave number structures, which do not propagate with the sun, lead to relatively fixed longitudinal patterns. This study leverages longitudinal variations observed from sun-synchronous orbit satellites, which offer consistent local time data, enabling the removal of solar illumination and photolysis effects, thereby allowing for a focused analysis on

25   nonmigrating diurnal variations (Oberheide and Forbes, 2008). This approach facilitates a clearer understanding of the stable tidal structures that modulate the MLT, distinguishing them from other factors such as solar-driven photochemistry.

   Exploiting the accumulation of continuous lidar observations, researchers have shown an increased interest in the diurnal variations of these metals and their possible driving mechanisms in recent decades. Clemesha et al. (1982, 2002) found that the diurnal variation of Na density was related to tidal winds at São José dos Campos (23°S, 46°W). In contrast, further analysis

30   found that the diurnal variation in Na was largely influenced by photochemistry rather than tidal forcing on the bottom side of the Na layer (States and Gardner, 1999; Yuan et al., 2012, 2019). Comparisons of lidar observations from the Chinese Meridian Project indicate that there are considerable regional differences in the Na diurnal cycle across China. The diurnal variations appear to be principally driven by photochemistry over Beijing (40.5°N, 116°E), while tidal modulations dominate over Wuhan (30.5°N, 114.6°E) (Gong et al., 2015; Xia et al., 2020a, b). These observations indicate that the mechanisms controlling the

35   diurnal variability of the Na layer are complex. The interplay between tides, solar-driven photochemistry, and atmospheric background conditions complicates the identification of a single controlling mechanism. Given these complexities and the limitations of point observations, our study utilized global satellite data and forward modelling to investigate the influence of nonmigrating tides on Na layer fluctuations in the MLT region and to explore the mechanisms which drive these fluctuations.

   In this study, we investigate the response of diurnal variations of atomic Na to nonmigrating diurnal tides using output

40   from the Specified Dynamics (SD) Whole Atmosphere Community Climate Model (WACCM), which is nudged by NASA's Modern-Era Retrospective Analysis for Research and Applications, Version 2 (MERRA-2) product (Molod et al., 2015). Owing to the characteristics of its sun-synchronous orbit, the Na density retrieved from the Optical Spectrograph and InfraRed Imaging System (OSIRIS) on the Odin satellite exhibits clear longitude variations, indicating the presence of tidal components. This integration of satellite observations and model simulations provides a novel approach to understanding the tidal influences on

45   the Na layer. Specifically, the correlation of the temperature nonmigrating diurnal tide and metal layer variability provides evidence for a mechanism for how temperature modulates the metal layer variation. Section 2 provides a detailed description of the model and observational data The results of the analysis are presented in section 3, with conclusions in Section 4.

2 Model Description and Data Analysis

2.1 Model Description

50 Our results are derived from a simulation of SD-WACCM (Smith et al., 2017; Yuan et al., 2019), a modified version of WACCM6 nudged to meteorological fields from the MERRA-2 analysis. WACCM6 is a high-top atmospheric model within the framework of the Community Earth System Model Version 2 (Gettelman et al., 2019), with 88 vertical levels up to approx-

imately 140 km altitude. The horizontal resolution of this simulation is $1.9° \times 2.5°$, and the time interval of the output data is 1 hr. This setup also includes the validated metal chemistry module for Na (Marsh et al., 2013) with updated rate coefficients from Plane et al. (2015).

WACCM is widely used in atmospheric tidal studies in the MLT region and compares satisfactorily with various observations (e.g., Chang et al., 2008; Lu et al., 2011, 2012; Davis et al., 2013; Ramesh and Smith, 2021). The WACCM model with Na, Fe, and K chemistry schemes has been successfully used to simulate the periodic characteristics of the MLT metal layers. For example, the teleconnections between metal layer variations and the solar cycle have been investigated by the model output and confirmed by parallel satellite observations (Dawkins et al., 2016; Wu et al., 2019). The simulated diurnal cycle of Fe, Na and K in WACCM compares favourably with lidar observations, except that the peak height of the modelled layers is 2-3 km lower than observations (Feng et al., 2015; Viehl et al., 2016; Yuan et al., 2019), which may be due to slow vertical transport caused by the unresolved waves in the gravity parametrization scheme (Yu et al., 2022). Due to the ability of this state-of-the-art model to simulate periodic diurnal changes in the metal layer close to observations, it is possible to investigate the response of the metal layers to nonmigrating diurnal tides.

2.2 Data Analysis

The Na layer observations measurements in the equatorial region (defined hereafter as 15°S-15°N) that are used here come from nearly ten years of Na number density measurements made by OSIRIS/Odin during 2004–2013 (Langowski et al., 2017). Odin is a limb-scanning satellite in a sun-synchronous orbit, with an ascending node at about 1800 local time (LT) and a descending node at about 0600 LT. The Na D-lines at 589 nm in the dayglow emission are predominantly produced by solar-stimulated resonance fluorescence of Na atoms. The limb-scanning measurements of the D-line emission, made by the OSIRIS spectrometer, are then converted into absolute Na atomic concentration profiles using the retrieval scheme of Gumbel et al. (2007). Hence, the Na observations are daytime only ($\sim$0600 and 1800 LT), which removes a potential photochemical day/night variation when analysing the diurnal tidal signal. Due to the severe lack of adequate data at the ascending node (1800 LT) over the equatorial latitudes, we mainly present the observation results of the descending node (0600 LT).

Using SD-WACCM data from 2004 to 2013, with a 1-hour time resolution, we extracted the amplitudes and phases of tides through a two-dimensional Fast Fourier Transform (2D FFT). The method is applied to the time-longitude series of Na, U, V, W, and T at each latitude and height level. In this paper, we limited our analysis to the three dominant tidal components: DW2 (Diurnal Westward Wavenumber 2), DE3 (Diurnal Eastward Wavenumber 3), and DS0 (Diurnal Stationary Tide), because there is much observational evidence showing that these are the most prominent components of the nonmigrating diurnal tides in the MLT region (Forbes et al., 2003; Wu et al., 2008; Zhang et al., 2010; Lu et al., 2011).

3 Results and Discussion

Figure 1 shows the longitude/altitude distribution of the composite monthly average equatorial Na density from OSIRIS/Odin observations between 2004 and 2013 at 0600 LT (descending node) and the corresponding WACCM model outputs for the same

85   period at 0600 LT for March, June, September, and December. The corresponding temperatures from WACCM are presented with contour lines in the right panels. As illustrated in Figure 1, the WACCM Na peak density ($\sim$4000 cm^{-3}) is approximately 30% higher than the observations, and the peak height ($\sim$ 90 km) is 2-3 km lower, which is consistent with the results reported in the previous studies (Feng et al., 2015; Viehl et al., 2016; Yuan et al., 2019; Yu et al., 2022). The Na density distributions from both the OSIRIS/Odin observations and WACCM exhibit a pronounced longitudinal variation. The Na number density

90   from OSIRIS/Odin and WACCM is much lower in March than in other months (June, September, and December).

    Although extracting tidal signals at a fixed local time is challenging, the total coverage at the same local time provides an excellent opportunity to show the longitudinal variations influenced by tidal components. In the left panels of Figure 1, the OSIRIS/Odin observations exhibit an apparent wave-3/wave-4 longitudinal structure in June, while there are only single or double maxima in other months. In the right panels of Figure 1, the WACCM model data show visible wave-2 or wave-3

95   patterns in June and September, and the other months exhibit more hybrid structures. It should be noted that the WACCM simulation and Odin observations are not expected to match precisely due to inherent differences in model assumptions, data resolution, and the specific physical processes represented. The longitudinal variation of Na density at the peak height ($\sim$ 90 km) in the WACCM is consistent with the temperature variation (contour lines) at the corresponding height (right panels of Figure 1). For example, each density maximum corresponds precisely to the temperature maximum in June. Specifically,

100   in June, the Na density peaks at around 4000 cm^{-3}, coinciding with temperature maxima of approximately 190 K. This longitudinal variation is suggested to be attributed to the tidal temperatures, where Na density is positively correlated with temperature (Plane et al., 1999, 2015; Wu et al., 2019). We also investigated the role of tidal winds (zonal and meridional winds, as well as vertical transport). We found no statistically significant relationship between these tidal winds and Na density (Fig. S1 in the Supplement).

105   Figure 2 shows the equatorial Na column abundance residuals at 0600 LT from the WACCM outputs (blue line) and OSIRIS/Odin observations (orange line), respectively. The residuals are obtained by subtracting the zonal mean data from the monthly mean column abundance profiles, which eliminates migrating tidal impacts and retains only perturbations due to nonmigrating tides. Although the Na peak heights and densities of the two datasets are different (Figure 1), their column abundance residuals are of the same order. Notably, the range of Na column abundance residuals (difference between the highest

110   and lowest values) is $\sim$1.0$\times$10^{9} cm^{-2}, indicating similar magnitudes of nonmigrating tidal influences in both datasets. The significant longitudinal variation is further supported in the Na column abundance residuals, and is also consistent with the Na concentration variations with longitude shown in Figure 1. In some months, the Na column abundance residuals from Odin and WACCM overlap significantly (e.g., February, March, July, and September), while in other months, they exhibit phase differences (e.g., May, August, November, and December). However, both distributions consistently display patterns of super-

115   imposed wave oscillations. As expected, the disturbances are particularly intense from January to February and from May to October, coinciding with the significant presence of nonmigrating tidal components (DW2 and DE3) during these months.

    Since Odin Na measurements were essentially limited to the same local time, this provides a rare opportunity to measure the longitudinal variations introduced by nonmigrating tides. However, extracting the relevant fluctuations in amplitude is challenging due to this observational limitation. Consequently, we will use the WACCM model results for quantitative analysis.
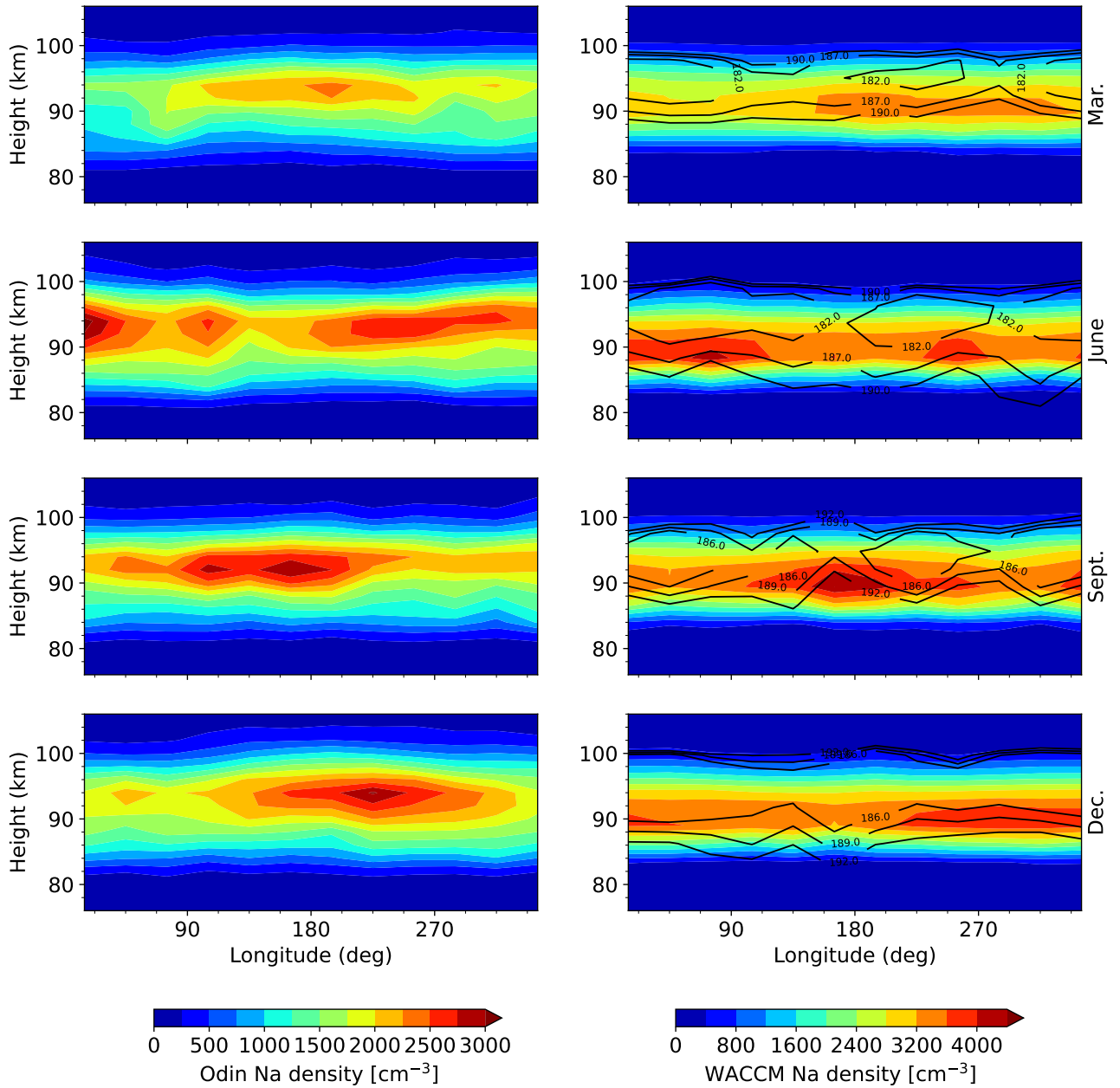
Figure 1. Composite monthly average Na density from OSIRIS/Odin observations (left), WACCM model output (right) over the equatorial region for March, June, September, and December. The Odin observations presented here were from the descending part of the orbit at 0600 LT for the years 2004 to 2013, and the WACCM results were for the same period at 0600 LT. Contour lines on right panels denote WACCM temperatures.

Figure 2. Composite monthly average equatorial Na column abundance residuals from Odin (orange line) and WACCM (blue line) with standard error bars for both datasets from 2004 to 2013.

Furthermore, SD-WACCM, constrained by MERRA-2 data below 60 km, is well-suited for investigating the mechanisms of tidal influence on the sodium layer.

Figure 3 shows the seasonal variation of the tidal amplitudes and phases of DW2, DE3 and DS0 for Na number density from WACCM over the equatorial region, with superposed contour lines of corresponding temperature tides. There are two peaks in the maximum Na density tidal amplitudes (left column in Figure 3). The primary peak amplitude of the Na density tidal variations ranges from 400 cm^{-3} to 500 cm^{-3}, occurring at 80-90 km, while the second peak altitude is ∼10 km higher with an amplitude that is about half that of the first peak. The magnitude of the DW2 and DE3 tidal amplitudes is comparable, but much stronger than those of DS0, which is consistent with their temperature tidal amplitudes at the corresponding heights. DW2 and DE3 exhibit peak amplitudes up to 500 cm^{-3}, whereas DS0 typically exhibits peak amplitudes around 350 cm^{-3}.

The seasonal distribution of the maxima/minima in the magnitude of the Na tidal amplitudes is generally consistent with the temperature component at the corresponding altitude, and the seasonal variations of the amplitude of the two vertical peaks are roughly synchronous. Generally, the response of the Na density to a 1 K change in tidal temperature is estimated to be 120 cm^{-3} at the primary peak height ($\sim$87 km). As shown in Figure 3, DW2 is comparable in most seasons, with the maximum occurring from September to November and the minimum in May; DE3 is strongest during June-October and less strong in April; and DS0 is prominent in July. This seasonal variation pattern is consistent with that of Forbes et al. (2003). Regarding the phase of Na density with that of temperature, their correlation varies with altitude, with a critical level of $\sim$90 km. Since the data covered almost a full solar cycle (2004-2013), our investigation extended to the impact of solar activity on the seasonal distribution of these nonmigrating tidal components and found that solar activity had no significant impact on the results (Figs. S2 and S3 in the Supplement).

The Pearson correlation coefficient distribution between the monthly variations of Na number density and those of temperature at the equatorial latitudes is presented in Figure 4 for these three components. Between 80 and 92 km, the three tidal components share a common feature: both amplitude and phase in Na density exhibit a significant positive correlation with temperature tides. This indicates that increases in temperature are generally accompanied by increases in Na density. In contrast, above 95 km, the Na tidal amplitude continues to be positively correlated with temperature, suggesting that temperature fluctuations still drive changes in Na density. However, the phase shows a marked negative correlation, indicating a phase shift where increases in temperature correspond to decreases in the Na density. This shift highlights a complex interaction between Na density and temperature at higher altitudes.

The altitude-dependent correlation of Na number density variations to temperature variations seems consistent with the study, which found that Na exhibits a positive correlation with the simulated temperature at approximately 90 km (Figure 10 in Plane et al. (1999), and Figure 2 in Wu et al. (2019)). Plane et al. (1999, 2015) provide a possible explanation for the correlation between metal atoms and temperature in the MLT region, and herein we give a brief summary. Over the height range $\sim$80-90 km, neutral chemistry dominates. The metal Na atoms are released from the reservoir $NaHCO_3$ by reaction with atomic H ($NaHCO_3 + H \rightarrow Na + H_2CO_3$); the rate coefficient has a positive activation energy (Plane et al., 2015) and so increases at higher temperatures. The explanation for the second peak altitude at $\sim$ 95 km is more complicated. The Na reservoir species here is Na^+. This is converted back to Na by recombination with N_2, followed by switching with CO_2 to form the $Na^+.CO_2$ which then undergoes dissociative electron recombination (Cox and Plane, 1998). The recombination reaction has a negative temperature dependence, and so is slower at higher temperature. Moreover, atomic O can disrupt the neutralization sequence by reacting with $Na^+.N_2$ to form NaO^+, which then reacts with a second O to reform Na^+. After examining the relationship between atomic O and temperature (Fig. S4 in the Supplement), we found that atomic O is positively correlated with temperature. Thus, Na should be less strongly correlated with temperature on the top-side of the layer (Plane et al., 1999). Indeed, Figure 4(b) shows that the Na phases of all three tidal components exhibit a significant anticorrelation with the temperature phase between 95 and 100 km, which is consistent with the anti-correlation of Na density and temperature above 96 km from pretvious lidar measurements and numerical simulations (Plane et al., 1999).
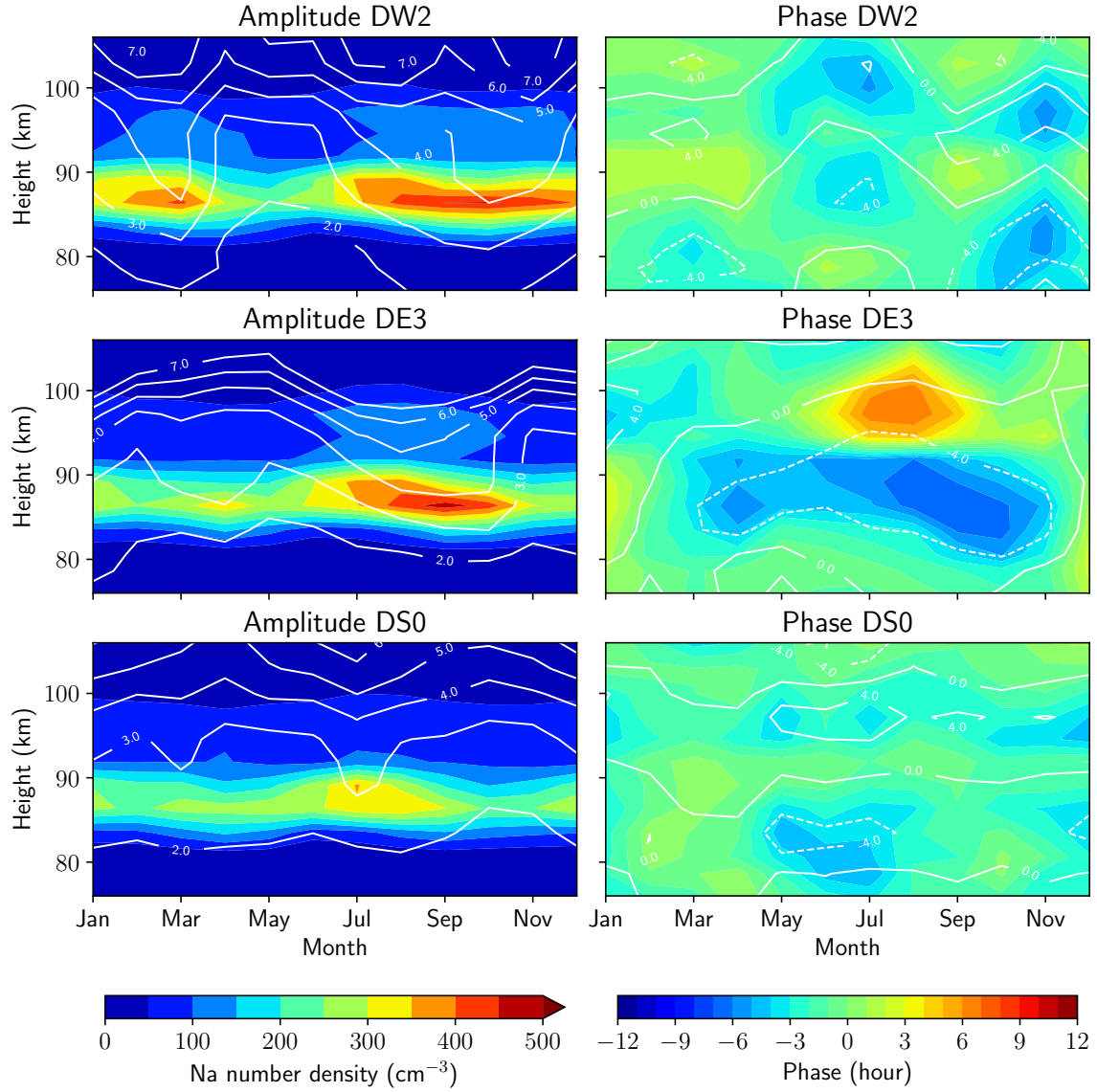
Figure 3. Seasonal variation of three nonmigrating diurnal tidal components of Na number density (color shading) and temperature (contours) for amplitudes (left panels) and phases (right panels) over the equatorial latitudes as a function of month and altitude.
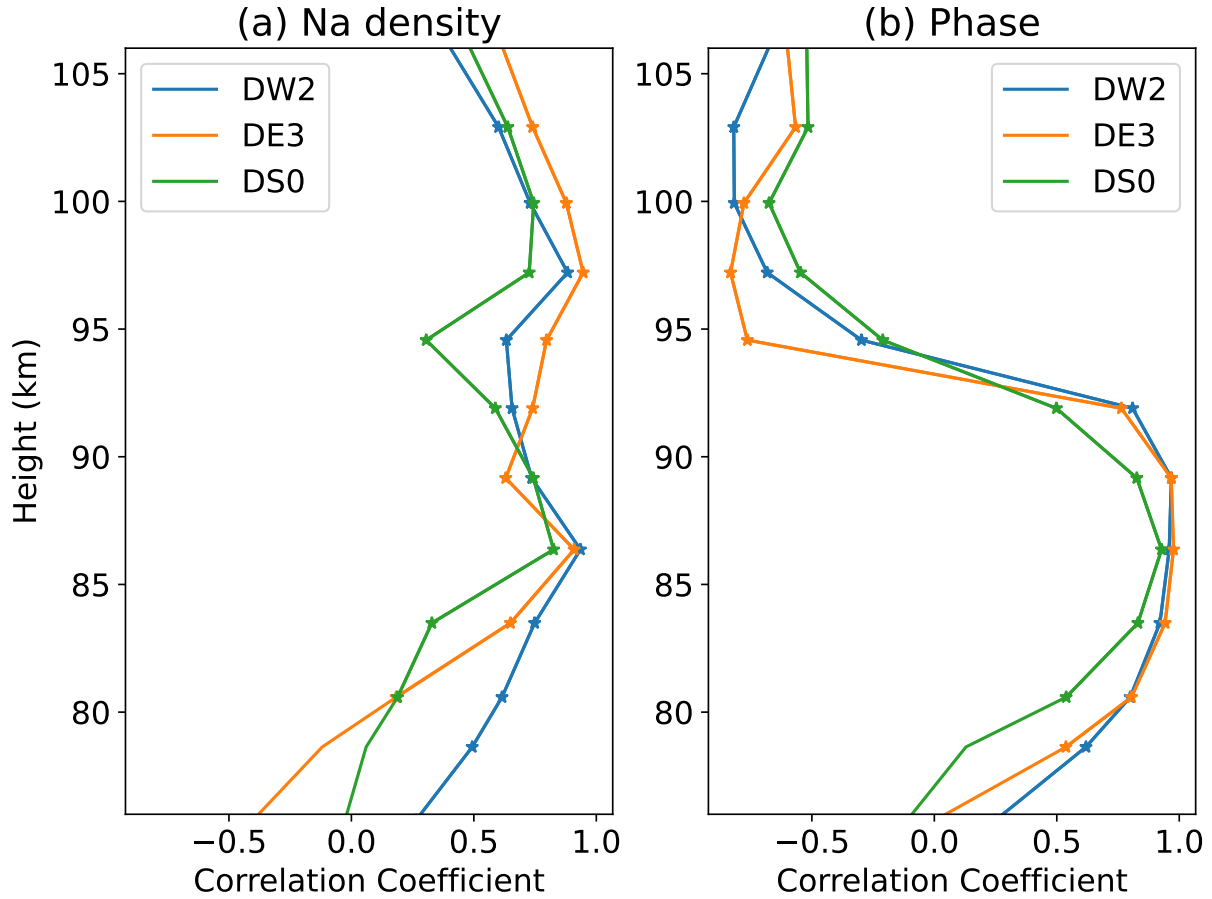
Figure 4. The Pearson correlation coefficient between Na number density and temperature variations for amplitudes (a) and phases (b) at the equatorial latitudes as a function of altitude (76–110 km). Those at 95% confidence levels are marked with asterisks.

Figure 5 illustrates the vertical profiles of the mean nonmigrating diurnal variation and diurnal variation from 2004-2013 at equatorial latitudes ($\pm15°$), and includes the mean Na density profile (left panel). It also shows their percentages relative to the mean Na density (right panel). The diurnal variation reaches its peak of around 900 cm^{-3} at approximately 90 km, aligning with the peak height of the Na density. In contrast, the nonmigrating diurnal variation has a mean peak amplitude of 350 cm^{-3}, occurring at a slightly lower altitude of $\sim$87 km, which is consistent with the findings shown in Figure 3. This peak amplitude of the nonmigrating diurnal tides in Na density represents $\sim$10% of the mean Na peak density (3500 cm^{-3}) and contribute $\sim$40% of the total diurnal variation in Na density. In this region, the remaining diurnal Na density variations may be due to the combined effects of migrating diurnal tides, photochemistry and non-tidal effects. More full diurnal cycle observations are required to investigate their contributions (States and Gardner, 1999; Yuan et al., 2012; Xia et al., 2020b). Above 95 km, the contributions of the nonmigrating diurnal tidal amplitude increases gradually to a maximum around 100 km of 25%, corresponding to the second peak height result shown in Figure 3. Interestingly, on the bottom side of the Na layer

(around 80 km), where photochemistry plays a major role, it can be inferred from the two percentages that the Na diurnal variation is comparable to the Na density, which is in good agreement with lidar observations (States and Gardner, 1999; Yuan et al., 2019; Xia et al., 2020b).
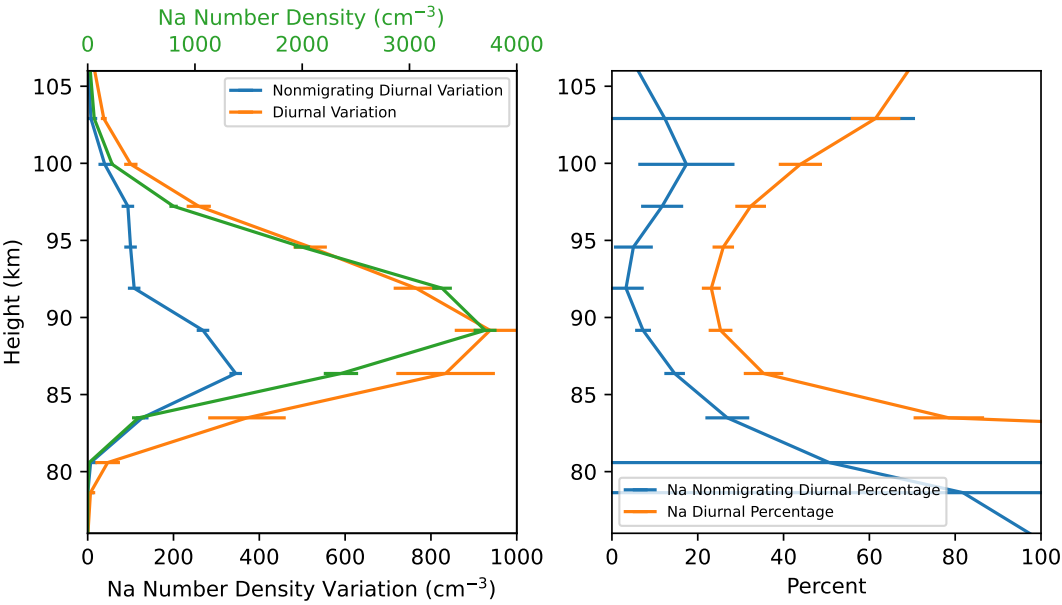
Figure 5. Vertical profiles of the 2004-2013 mean nonmigrating diurnal variation (blue) and diurnal variation (orange) at equatorial latitudes (left panel), and their percentages relative to the mean Na density (right panel). The green profile represents the mean Na density.

4 Conclusions

The nonmigrating diurnal tidal variation of the metal layers in the MLT region has been investigated using data from OSIRIS/Odin observations and the SD-WACCM model with added metal chemistry. Whereas previous studies focused on the influence of photochemistry on the diurnal variations in Na density on the top and bottom sides of the layer, to the best of our knowledge this is the first time that the nonmigrating diurnal tidal signal of a metal layer has been investigated. The present study found the following features: (1) the Na density exhibits longitudinal variations, indicating tidal components in both datasets, although there are differences between the two datasets which vary month-to-month; (2) there is a significant relationship between the nonmigrating diurnal variation in Na density and the corresponding temperature tidal signal, rather than with dynamics such as the wind tides; (3) the mean amplitude of the nonmigrating diurnal variation in Na density at the equatorial latitudes is $\sim$350 cm^{-3} at 87 km, accounting for 10% of the mean Na number density and contributing $\sim$40% of the total diurnal variation of Na; (4) below 90 km, the amplitude and phase of the three nonmigrating diurnal tidal components in Na density show a significant positive correlation with the temperature tides, while above 95 km, the phase shows a negative correlation.

Previous research has established the diurnal variation on the top and bottom sides of three metal layers (Na, K, and Fe) by lidar and modelling (e.g., States and Gardner, 1999; Yuan et al., 2012; Yu et al., 2012; Feng et al., 2015; Yuan et al., 2019; Xia et al., 2020a). This study is the first to extract nonmigrating diurnal tidal signals from diurnal variations through a global atmospheric metal layer model, and a significant magnitude is found around the Na layer peak. In the near future, the construction and continuous observation using high-precision lidars at the same latitude, which is part of the Chinese of the Meridian Project Phase II, will provide new opportunities to investigate and understand nonmigrating tidal variations in the metal layers.

Code and data availability. The SD-WACCM model output data presented in this study is available at Wu et al. (2024). The WACCM6 model code can be accessed from https://www.cesm.ucar.edu/working-groups/whole-atmosphere. The derived OSIRIS/ODIN Na data (Dawkins et al., 2016) presented in this study is available at Wu et al. (2023).

Supplement. The supplement related to this article is available online at:

Author contributions. J. W. in close collaboration with W. F., J. M. C. P. and D. R. M. designed the experiment, ran the WACCM model, J. W. performed the data analysis, and prepared the manuscript. W. F., X.X., and J. M. C. P. contributed to the interpretation of results and the writing of the manuscript.

Competing interests. At least one of the (co-)authors is a member of the editorial board of Atmospheric Chemistry and Physics.

Acknowledgements. This work was supported by the National Key R&D Program of China (Grant No. 2022YFF0503703), the National Natural Science Foundation of China (42125402, 42188101, 42374183, and 42074181), the Project of Stable Support for Youth Team in Basic Research Field, CAS (YSBR-018). J. W. was funded by the foundation of the Fundamental Research Funds for the Central Universities (Grant No. WK3420000020). W. F., J. M. C. P. and D. R. M. are supported by the jointly funded project by the USA National Science Foundation's Directorate of Geosciences (NSFGEO) and the UK National Environment Research Council (grant no. NE/T006749/1). W. F. is partly funded by NCAS Visiting Scientist Programme. The numerical calculations in this paper were undertaken on the supercomputing system in the Supercomputing Center of the University of Science and Technology of China.

References

Chang, L., Palo, S., Hagan, M., Richter, J., Garcia, R., Riggin, D., and Fritts, D.: Structure of the migrating diurnal tide in the Whole Atmosphere Community Climate Model (WACCM), Advances in Space Research, 41, 1398–1407, https://doi.org/10.1016/j.asr.2007.03.035, 2008.

Clemesha, B. R., Simonich, D. M., Batista, P. P., and Kirchhoff, V. W. J. H.: The diurnal variation of atmospheric sodium, Journal of Geophysical Research: Space Physics, 87, 181–186, https://doi.org/10.1029/JA087iA01p00181, 1982.

Clemesha, B. R., Batista, P. P., and Simonich, D. M.: Tide-induced oscillations in the atmospheric sodium layer, Journal of Atmospheric and Solar-Terrestrial Physics, 64, 1321–1325, https://doi.org/10.1016/s1364-6826(02)00115-3, 2002.

Cox, R. M. and Plane, J. M. C.: An ion-molecule mechanism for the formation of neutral sporadic Na layers, Journal of Geophysical Research: Atmospheres, 103, 6349–6359, https://doi.org/10.1029/97JD03376, 1998.

Davis, R. N., Du, J., Smith, A. K., Ward, W. E., and Mitchell, N. J.: The diurnal and semidiurnal tides over Ascension Island (8°S, 14°W) and their interaction with the stratospheric quasi-biennial oscillation: studies with meteor radar, eCMAM and WACCM, Atmospheric Chemistry and Physics, 13, 9543–9564, https://doi.org/10.5194/acp-13-9543-2013, 2013.

Dawkins, E. C. M., Plane, J. M. C., Chipperfield, M. P., Feng, W., Marsh, D. R., Höffner, J., and Janches, D.: Solar cycle response and long-term trends in the mesospheric metal layers, Journal of Geophysical Research: Space Physics, 121, 7153–7165, https://doi.org/10.1002/2016JA022522, 2016.

Feng, W., Marsh, D. R., Chipperfield, M. P., Janches, D., Hoffner, J., Yi, F., and Plane, J. M. C.: A global atmospheric model of meteoric iron, Journal of Geophysical Research-Atmospheres, 118, 9456–9474, 2013.

Feng, W., Hoffner, J., Marsh, D. R., Chipperfield, M. P., Dawkins, E. C. M., Viehl, T. P., and Plane, J. M. C.: Diurnal variation of the potassium layer in the upper atmosphere, Geophysical Research Letters, 42, 3619–3626, https://doi.org/10.1002/2015GL063718, 2015.

Forbes, J. M., Zhang, X., Talaat, E. R., and Ward, W.: Nonmigrating diurnal tides in the thermosphere, Journal of Geophysical Research: Space Physics, 108, https://doi.org/10.1029/2002ja009262, 2003.

Gettelman, A., Mills, M. J., Kinnison, D. E., Garcia, R. R., Smith, A. K., Marsh, D. R., Tilmes, S., Vitt, F., Bardeen, C. G., McInerny, J., Liu, H.-L., Solomon, S. C., Polvani, L. M., Emmons, L. K., Lamarque, J.-F., Richter, J. H., Glanville, A. S., Bacmeister, J. T., Phillips, A. S., Neale, R. B., Simpson, I. R., DuVivier, A. K., Hodzic, A., and Randel, W. J.: The Whole Atmosphere Community Climate Model Version 6 (WACCM6), Journal of Geophysical Research: Atmospheres, 124, 12 380–12 403, https://doi.org/10.1029/2019JD030943, 2019.

Gong, S., Yang, G., Cheng, X., Gong, S., Xu, J., Li, F., Gong, W., and Wang, J.: Lidar observation campaigns on diurnal variations of the sodium layer in Beijing and Wuhan, China, Science China-Earth Sciences, 58, 1377–1386, https://doi.org/10.1007/s11430-015-5099-1, 2015.

Gumbel, J., Fan, Z. Y., Waldemarsson, T., Stegman, J., Witt, G., Llewellyn, E. J., She, C.-Y., and Plane, J. M. C.: Retrieval of global mesospheric sodium densities from the Odin satellite, Geophysical Research Letters, 34, https://doi.org/10.1029/2006GL028687, 2007.

Langowski, M. P., von Savigny, C., Burrows, J. P., Fussen, D., Dawkins, E. C. M., Feng, W., Plane, J. M. C., and Marsh, D. R.: Comparison of global datasets of sodium densities in the mesosphere and lower thermosphere from GOMOS, SCIAMACHY and OSIRIS measurements and WACCM model simulations from 2008 to 2012, Atmospheric Measurement Techniques, 10, 2989–3006, https://doi.org/10.5194/amt-10-2989-2017, 2017.

Li, X., Ren, Z., Cao, J., Yu, Y., Wang, Y., and Zhou, X.: Comparative Study of the Variability of the Non-Migrating Tide DE3 Using WACCM-X Simulations and TIMED/SABER Observations, Earth and Space Science, 9, e2021EA002 117, https://doi.org/10.1029/2021EA002117, 2022.

Lu, X., Liu, A. Z., Oberheide, J., Wu, Q., Li, T., Li, Z., Swenson, G. R., and Franke, S. J.: Seasonal variability of the diurnal tide in the mesosphere and lower thermosphere over Maui, Hawaii (20.7°N, 156.3°W), Journal of Geophysical Research: Atmospheres, 116, https://doi.org/10.1029/2011jd015599, 2011.

Lu, X., Liu, H.-L., Liu, A. Z., Yue, J., McInerney, J. M., and Li, Z.: Momentum budget of the migrating diurnal tide in the Whole Atmosphere Community Climate Model at vernal equinox, Journal of Geophysical Research: Atmospheres, 117, D07 112, https://doi.org/10.1029/2011JD017089, 2012.

Marsh, D. R., Janches, D., Feng, W., and Plane, J. M. C.: A global model of meteoric sodium, Journal of Geophysical Research-Atmospheres, 118, 11 442–11 452, 2013.

Molod, A., Takacs, L., Suarez, M., and Bacmeister, J.: Development of the GEOS-5 atmospheric general circulation model: evolution from MERRA to MERRA2, Geoscientific Model Development, 8, 1339–1356, https://doi.org/10.5194/gmd-8-1339-2015, 2015.

Oberheide, J. and Forbes, J. M.: Thermospheric nitric oxide variability induced by nonmigrating tides, Geophysical Research Letters, 35, 814, https://doi.org/10.1029/2008GL034825, 2008.

Plane, J. M. C., Gardner, C. S., Yu, J., She, C. Y., Garcia, R. R., and Pumphrey, H. C.: Mesospheric Na layer at 40°N: Modeling and observations, Journal of Geophysical Research: Atmospheres, 104, 3773–3788, https://doi.org/10.1029/1998JD100015, 1999.

Plane, J. M. C., Feng, W., and Dawkins, E. C.: The mesosphere and metals: chemistry and changes, Chem Reviews, 115, 4497–541, https://doi.org/10.1021/cr500501m, 2015.

Ramesh, K. and Smith, A. K.: Long-Term Variability and Tendencies in Non-Migrating Diurnal Tide From WACCM6 Simulations During 1850–2014, Journal of Geophysical Research: Space Physics, 126, e2020JA028 904, https://doi.org/10.1029/2020JA028904, 2021.

Smith, A. K.: Global dynamics of the MLT, Surveys in Geophysics, 33, 1177–1230, 2012.

Smith, A. K., Pedatella, N. M., Marsh, D. R., and Matsuo, T.: On the Dynamical Control of the Mesosphere–Lower Thermosphere by the Lower and Middle Atmosphere, Journal of the Atmospheric Sciences, 74, 933 – 947, https://doi.org/10.1175/JAS-D-16-0226.1, 2017.

States, R. J. and Gardner, C. S.: Structure of the mesospheric Na layer at 40°N latitude: Seasonal and diurnal variations, Journal of Geophysical Research-Atmospheres, 104, 11 783–11 798, https://doi.org/10.1029/1999jd900002, 1999.

Viehl, T. P., Plane, J. M. C., Feng, W., and Höffner, J.: The photolysis of FeOH and its effect on the bottomside of the mesospheric Fe layer, Geophysical Research Letters, 43, 1373–1381, https://doi.org/10.1002/2015gl067241, 2016.

Wu, J., Feng, W., Xue, X., Marsh, D. R., Plane, J. M. C., and Dou, X.: The 27-Day Solar Rotational Cycle Response in the Mesospheric Metal Layers at Low Latitudes, Geophysical Research Letters, 46, 7199–7206, https://doi.org/10.1029/2019gl083888, 2019.

Wu, J., Feng, W., Xue, X., Marsh, D. R., and Plane, J. M. C.: Odin/OSIRIS Na data, https://doi.org/10.17632/k75wsc5p88.3, 2023.

Wu, J., Feng, W., Xue, X., Marsh, D. R., and Plane, J. M. C.: Simulation data of 'Effects of Nonmigrating Diurnal Tides on the Na Layer in the Mesosphere and Lower Thermosphere', https://doi.org/10.5281/zenodo.12700538, 2024.

Wu, Q., Ortland, D. A., Killeen, T. L., Roble, R. G., Hagan, M. E., Liu, H.-L., Solomon, S. C., Xu, J., Skinner, W. R., and Niciejewski, R. J.: Global distribution and interannual variations of mesospheric and lower thermospheric neutral wind diurnal tide: 2. Nonmigrating tide, Journal of Geophysical Research: Space Physics, 113, https://doi.org/10.1029/2007ja012543, 2008.

Xia, Y., Cheng, X., Li, F., Yang, Y., Jiao, J., Xun, Y., Li, Y., Du, L., Wang, J., and Yang, G.: Diurnal variation of atmospheric metal Na layer and nighttime top extension detected by a Na lidar with narrowband spectral filters at Beijing, China, Journal of Quantitative Spectroscopy and Radiative Transfer, 255, 107 256, https://doi.org/10.1016/j.jqsrt.2020.107256, 2020a.

285   Xia, Y., Cheng, X., Li, F., Yang, Y., Lin, X., Jiao, J., Du, L., Wang, J., and Yang, G.: Sodium lidar observation over full diurnal cycles in Beijing, China, Applied Optics, 59, 1529–1536, https://doi.org/10.1364/AO.382077, 2020b.

Yu, B., Xue, X., Scott, C. J., Jia, M., Feng, W., Plane, J. M. C., Marsh, D. R., Hedin, J., Gumbel, J., and Dou, X.: Comparison of middle- and low-latitude sodium layer from a ground-based lidar network, the Odin satellite, and WACCM–Na model, Atmospheric Chemistry and Physics, 22, 11 485–11 504, https://doi.org/10.5194/acp-22-11485-2022, 2022.

290   Yu, Z., Chu, X., Huang, W., Fong, W., and Roberts, B. R.: Diurnal variations of the Fe layer in the mesosphere and lower thermosphere: Four season variability and solar effects on the layer bottomside at McMurdo (77.8°S, 166.7°E), Antarctica, Journal of Geophysical Research: Atmospheres, 117, https://doi.org/10.1029/2012jd018079, 2012.

Yuan, T., She, C. Y., Kawahara, T. D., and Krueger, D. A.: Seasonal variations of midlatitude mesospheric Na layer and their tidal period perturbations based on full diurnal cycle Na lidar observations of 2002–2008, Journal of Geophysical Research: Atmospheres, 117,
295   https://doi.org/10.1029/2011JD017031, 2012.

Yuan, T., Feng, W., Plane, J. M. C., and Marsh, D. R.: Photochemistry on the bottom side of the mesospheric Na layer, Atmospheric Chemistry and Physics, 19, 3769–3777, https://doi.org/10.5194/acp-19-3769-2019, 2019.

Zhang, X., Forbes, J. M., and Hagan, M. E.: Longitudinal variation of tides in the MLT region: 1. Tides driven by tropospheric net radiative heating, Journal of Geophysical Research: Space Physics, 115, https://doi.org/10.1029/2009ja014897, 2010.